Accepted Manuscript

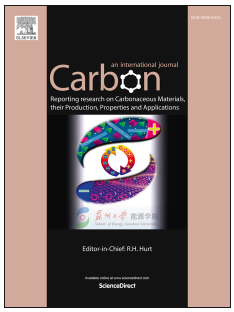

Template-induced self-activation route for nitrogen-doped hierarchically porous carbon spheres for electric double layer capacitors

Hongshuai Guo, Bing Ding, Jie Wang, Yadi Zhang, Xiaodong Hao, Langyuan Wu, Yufeng An, Hui Dou, Xiaogang Zhang

PII: S0008-6223(18)30440-8

DOI: 10.1016/j.carbon.2018.04.079

Reference: CARBON 13116

To appear in: *Carbon*

Received Date: 8 December 2017

Revised Date: 19 April 2018

Accepted Date: 25 April 2018

Please cite this article as: H. Guo, B. Ding, J. Wang, Y. Zhang, X. Hao, L. Wu, Y. An, H. Dou, X. Zhang, Template-induced self-activation route for nitrogen-doped hierarchically porous carbon spheres for electric double layer capacitors, *Carbon* (2018), doi: 10.1016/j.carbon.2018.04.079.

Template-Induced Self-Activation Route for Nitrogen-Doped Hierarchically Porous Carbon Spheres for Electric Double Layer Capacitors

Hongshuai Guo, Bing Ding, Jie Wang, Yadi Zhang, Xiaodong Hao, Langyuan Wu, Yufeng An, Hui Dou and Xiaogang Zhang[*]

Jiangsu Key Laboratory of Electrochemical Energy Storage Technologies, College of Materials Science and Engineering, Nanjing University of Aeronautics and Astronautics, Nanjing, 210016, P.R. China.

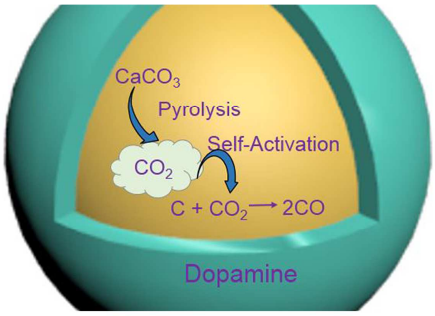

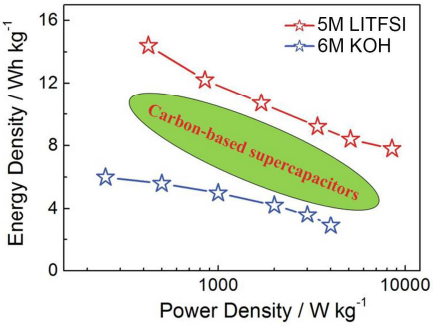

[*]Corresponding author. Tel.: +86 025 52112918; Fax: +86 025 52112626.

E-mail address: *azhangxg@nuaa.edu.cn* (Prof. X.G. Zhang).

Template-Induced Self-Activation Route for Nitrogen-Doped Hierarchically Porous Carbon Spheres for Electric Double Layer Capacitors

Hongshuai Guo, Bing Ding, Jie Wang, Yadi Zhang, Xiaodong Hao, Langyuan Wu, Yufeng An, Hui Dou and Xiaogang Zhang[*]

Jiangsu Key Laboratory of Electrochemical Energy Storage Technologies, College of Materials Science and Engineering, Nanjing University of Aeronautics and Astronautics, Nanjing, 210016, P.R. China.

ABSTRACT: The synthesis of highly nitrogen-doped hierarchical carbon spheres (NPCS) is reported. The NPCS with pomegranate-like nanostructure were prepared by the $CaCO_3$ spheres template-induced self-activation route with dopamine as the carbon precursor. The template-induced self-activation mechanism was carefully investigated by controlling experiment conditions and thermogravimetric analyses combined with mass spectrometry. Under the optimized conditions, the as-prepared NPCS demonstrate large specific area (up to 1984 $m^2\ g^{-1}$) and high level of nitrogen (N, 7.57%) doping. Electrochemical evaluations indicate that the energy density of NPCS-based EDLC devices can reach 6.2 and 14.4 Wh kg^{-1} in 6 M KOH electrolyte and aqueous concentrated electrolyte (5 M LiTFSI), respectively. This work provides a novel approach for preparing nanoporous carbon materials with hierarchical

[*]Corresponding author. Tel.: +86 025 52112918; Fax: +86 025 52112626.

E-mail address: *azhangxg@nuaa.edu.cn* (Prof. X.G. Zhang).

porosity and well-defined nanostructure.

1. Introduction

Supercapacitors, as one of advanced energy storage devices, have attracted tremendous attentions because of their high power density, short charging/discharging time, long cycle life and high safety [1-5]. Electric double layer capacitors (EDLCs) present most of commonly applied supercapacitors today, which hold promise for a wide range of applications, including hybrid electric vehicles, portable electronics and load leveling. However, compared with secondary batteries, EDLCs show lower energy density because the energy storage is based on electrical double layer charge accumulation at the electrolyte-electrode interface [6-9]. As known, porous carbon materials are widely used electrode materials for EDLCs. The electrochemical double layer capacitive performances of carbon electrode are highly associated with the surface area as well as the electronic/ionic transport kinetics. Apart from surface area, recent achievements have demonstrated that pore size distribution (PSD) is also a crucial factor on the capacitance and rate performance of carbon electrode [10-13]. In general, according to the pore size, the pore is divided into micropore (< 2 nm), mesopore (2-50 nm) and macropore (> 50 nm). Micropores contribute to the much surface area providing the capacitance but usually result in sluggish ion transportation and poor power capability. Mesopores are benefit for high accessibility for electrolyte and rate capability [14-17]. Therefore, carbon materials with well-controlled micro-

and meso-pores distribution, *e.g.* hierarchically porous carbon, are highly desired to realize high power and energy density of EDLC [18-23].

Various hierarchically porous carbon with different nanostructure and controllable meso/macroporous structure have been constructed by combining different hard templates [24-28] and soft templates [29-31]. Zhao and *co*-workers synthesized a series controllable meso/macroporous structure carbon by using dual-templating method (silica colloidal crystals as hard template and F127 as soft template). The obtained porous carbon exhibit large specific surface area (760 m^2 g^{-1}), high pore volume (1.25 cm^3 g^{-1}) and tunable macroporous size (from 230 to 430 nm) [32]. However, it is difficult for template method to pursue ultrahigh surface area while constructing well-balanced macro-, meso-, and micro-porosity, without combining post-activation. Traditional chemical/physical activation methods remain formidable challenge to pursuit of ultrahigh surface area while maintaining definite nanostructure, because the extensive creation of pores made by activator will undoubtedly damage the nanostructures [33]. In addition, it is time-consuming and harmful to remove some hard templates (like SiO_2). Therefore, a simple, cost-efficient and environment-friendly preparation method to construct controllable hierarchically porous structure is urgently needed.

In this work, $CaCO_3$ spheres template-induced self-activation route was developed for preparing nitrogen-doped hierarchically porous carbon spheres (NPCS). This method combines the advantages of hard template method and physical activation

method. As a result, the as-prepared NPCS materials exhibit well-defined pomegranate-like nanostructure as well as large specific surface area (up to 1984 m^2 g^{-1}), particular pore size distribution and high level of nitrogen doping (7.57%). Electrochemical evaluations indicate that the energy density of NPCS-based EDLC devices can reach 6.2 and 14.4 Wh kg^{-1} in 6 M KOH electrolyte and aqueous concentrated electrolyte (5 M LiTFSI), respectively. Compared with other hard template method (such as SiO_2 and polystyrene colloid spheres), the template-induced self-activation method described in this work provide an easy and effective approach for designing and preparation of nanoporous carbon materials with hierarchical porosity and well-defined nanostructure. This route could also be extended to prepare hierarchically porous carbon materials for other applications, such as batteries and catalysts.

2. Experimental

2.1 Materials Synthesis

2.1.1 *Synthesis of $CaCO_3$ spheres template*

The spherical $CaCO_3$ spheres template was prepared according to previous method described in the literature with some modifications [34]. The $CaCl_2 \cdot 2H_2O$ (0.0735 g) was added into 100 mL soluble starch (0.2500 g) solution. After stirring for about 1 h. 150 mL of Na_2CO_3 (0.05 M) aqueous solution was slowly dropped into above aqueous solution. After reaction for 12 h, the product was collected by centrifugation and carefully washed by water and ethanol for three times. The product was then

dried at 60 °C in oven for one night.

2.1.2 *Synthesis of NPCS and N-doped carbon spheres (NCS)*

Firstly, 0.2 g $CaCO_3$ spheres template was added to the tris-buffer (150 mL, pH = 8.5), then 0.2 g dopamine was slowly added. After stirring for 24 h, the $CaCO_3$@PDA particles were collected by centrifugation. The NPCS were obtained by further carbonization of the $CaCO_3$@PDA at 800 °C for 2 h in nitrogen (N_2) atmosphere and washing with HCl aqueous solution. By controlling the decomposition rate of $CaCO_3$ template, the $CaCO_3$@PDA composite were heated under different heating rate of 5 and 10 °C min^{-1} from 600 to 800 °C and the obtained carbon materials were marked as NPCS-1 and NPCS-2, respectively.

For synthesis of NCS, the $CaCO_3$@PDA samples were carbonized under N_2 atmosphere at 500 °C (lower than the pyrolysis temperature of $CaCO_3$) for 1 h with a heating rate of 5 °C min^{-1}, then the $CaCO_3$ was removed by washing with HCl aqueous solution and deionized water respectively. The obtained carbon spheres were completely carbonized at 800 °C with a heating rate of 5 °C min^{-1}. The NCS was obtained.

2.2 Materials Characterization

The morphologies of all the samples were characterized by scanning electron microscope (SEM Hitachi S-4800I) and transmission electron microscope (TEM FEI Tecnai G2F20). The X-ray diffraction (XRD) patterns were recorded on Bruker D8 Advance X-ray diffractor meter using Cu Kα (λ=0.154178 nm) radiation at a scanning

rate of 5° min^{-1}. Thermogravimetric analyses combined with mass spectrometry were performed on a NETZSCH STA4094C. The X-ray photoelectron spectroscopy (XPS) analysis was performed on a Perkin-Elmer PHI 550 spectrometer with Al Ka (1486.6 eV) as the X-ray source. The nitrogen adsorption-desorption isotherms of three samples were tested using Micromeritics BK122T-B analyzer. The specific surface area was calculated according to the BET theory and the pore size distributions (PSD) were derived from non-local density functional theory (NLDFT) model. Raman spectra was performed using the HORIBA Scientific LabRAM HR Raman spectrometer system under a 532.4 nm laser.

2.3 Electrochemical Measurements

All electrochemical measurements were carried out on a CHI 660C electrochemical workstation system (Chenhua, Shanghai). The EIS was performed in the frequency range of 0.01 Hz to 100 kHz. The cycle life was tested by LAND CT2001A electrochemical workstation. The working electrodes were prepared by mixing active material (3 mg), acetylene black (0.6 mg) and polytetrafluoroethylene (0.6 mg) binder, then blending the mixture completely and rolling into a paste. The foamed Ni grids was used as current collector in 6 M KOH aqueous solution, and stainless steels were used as current collector in 5 M LiTFSI aqueous solution. The paste was coated on the current collector by pressing under a pressure of 10 MPa.

In the three-electrode system, the specific capacitance (C) was calculated as:

$$C = (I\Delta t)/(m\Delta V) \quad (1)$$

where I is the current (A), Δt is the discharge time (s), m is the mass of active material (g) and ΔV represents the discharge potential window (V).

In the two-electrode system, the specific capacitance (C_s) of the electrode was calculated:

$$C_s = (4I\Delta t) / (m\Delta V) \quad (2)$$

where I is the current (A), Δt is the discharge time (s), m is the total mass of both carbon electrodes (g) and ΔV represents the cell voltage (V).

The gravimetric energy density (E) and power density (P) of device were calculated using the following formulas:

$$E = CV^2 / 2 \quad (3)$$

$$P = E / \Delta t \quad (4)$$

where C is the capacitance of the device, V is the operating voltage and Δt is the discharge time (s).

3. Results and discussions

The preparation route is schematically present in Figure 1. As shown in Figure 1a, $CaCO_3$ spheres assembled with inter-connected $CaCO_3$ nanoparticles are used as template. The dopamine polymerizes on each $CaCO_3$ nanoparticle to form $CaCO_3$@PDA composite. After carbonization and removing template, $CaCO_3$@PDA particles are converted to hollow carbon units, which are combined together into a

nitrogen-doped hierarchically porous carbon network. More importantly, degradation products of $CaCO_3$ nanoparticle are CO_2 and CaO. CO_2 could physically etch the carbon network and thus create abundant pores (Figure 1b) [35-37]. And the CaO has catalytic activity, which can reduce the activation energy of the reaction between CO_2 and carbon network, leading to the development of porosity. The CO_2 producing rate could be easily controlled by adjusting the heating rate. Different CO_2 producing rate result a different activation time and rate, realizing the controllable distribution of micro/mesopores. The introduction of nitrogen element can effectively improve the wettability of carbon materials and provide considerable contribution of the pseudocapacitance, improving the capacitance of carbon materials.

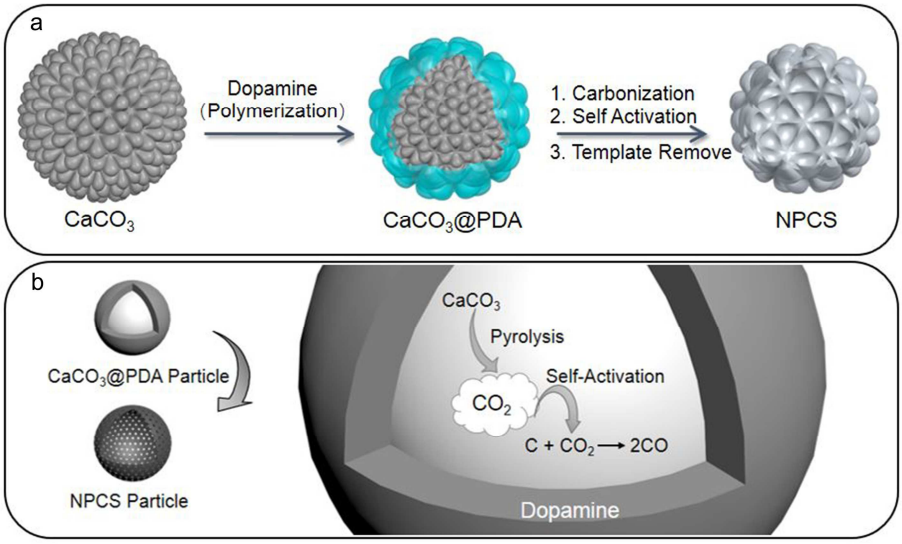

Figure 1. Schematic illustration for preparation of NPCS.

As shown in Figure 2a and S1a, the as-prepared $CaCO_3$ spheres show uniform and

pomegranate-like morphology with a diameter ~400-600 nm. The $CaCO_3$ spheres possess rough surface and are assembled by large amounts of nanocapsules (inset of Figure 2a). The TEM image (Figure S1b) indicates $CaCO_3$ spheres are assembled by large amounts of nanocapsules with a size of 30-70 nm. It can be seen that there are many gaps between nanocapsules which can provide space for infiltration of dopamine during the self-polymerization. As shown in Figure S1c, the $CaCO_3$@PDA still keeps the sphere morphology of $CaCO_3$. And, TEM image of $CaCO_3$@PDA (Figure S1d) exhibits a tight structure without gaps, indicating that dopamine can penetrate into the inner space of the $CaCO_3$ spheres to perform self-polymerization on each nanoparticle of $CaCO_3$. After heat treatment at 800 $^{\circ}$C with a heating rate of 5 $^{\circ}$C min^{-1} and template removing process, the $CaCO_3$@PDA converted to NPCS-1. As revealed in the SEM image of NPCS-1 (Figure 2b), it can be seen that the NPCS-1 exhibits rough surface and maintains the sphere morphology inherited from $CaCO_3$ spheres template without any structure collapse. TEM images (Figure 2c, e) indicate that NPCS-1 exhibits a uniform pomegranate-like microtopography, and there are many carbon sheets cross-linked in the inside of NPCS-1. The HRTEM image of NPCS-1 (in Figure 2d) indicates that the NPCS-1 belongs to the amorphous carbon. Elemental mappings (Figure 2f, g) were conducted to determine the element distribution of NPCS-1. It can be seen that C and N elements are uniformly distributed in the pomegranate-like carbon spheres. As shown in thermogravimetric (TG) analysis of $CaCO_3$ spheres (Figure S4). It can be found that $CaCO_3$ spheres

begin to decompose at about 600 °C and mainly decompose between 600 and 800 °C. Therefore, in order to evaluate the influence of the different CO_2 producing rate and template self-activation to porous structure, we carbonized the $CaCO_3$@PDA at 800 °C with a heating rate of 10 °C min^{-1} from 600 to 800 °C. The sample is denoted NPCS-2. And the N-doped carbon sphere (NCS) without $CaCO_3$ self-activation was prepared from pomegranate-like microtopography PDA sphere precursor. And as shown in Figure S2, the NPCS-2 and NCS have the similar size and rough surface sphere morphology as NPCS-1. That indicates the different heating rate and preliminary template removing process will not influence the sphere morphology.

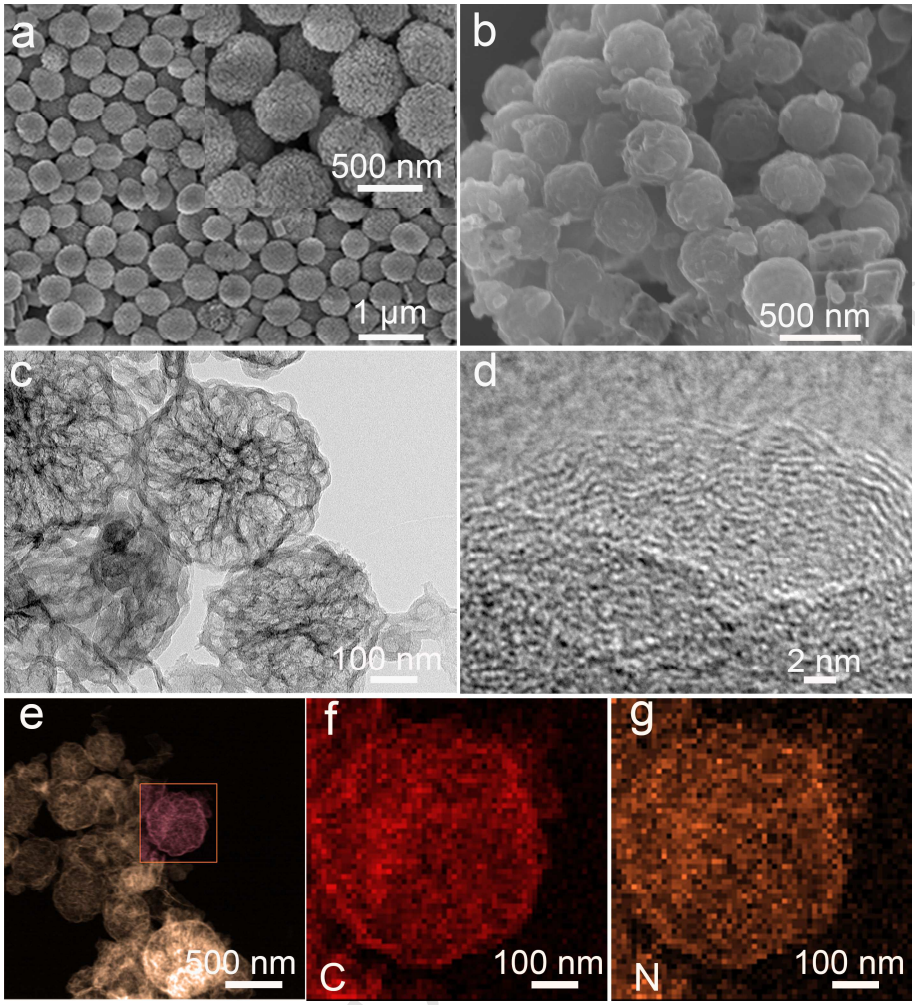

Figure 2. SEM images of (a) $CaCO_3$ spheres (The inset shows the high magnification SEM image of $CaCO_3$ spheres) and (b) NPCS-1. (c, e) TEM images and (d) HRTEM image of NPCS-1. (g, f) mapping images (C, N) of NPCS-1.

As shown in Figure S3, the typical calcite crystal of $CaCO_3$ spheres were completely transformed into the CaO crystal after heat treatment at 800 $^{\circ}$C. The XRD pattern of NPCS-1 shows two weak broad peaks, indicating it is amorphous structure. The detailed decomposition process of $CaCO_3$@PDA can be analyzed with

thermogravimetric analysis-mass spectrometry (TG-MS) analysis during the heat treatment at heating rate of 5 and 10 °C min^{-1} (Figure S5 and Table S1). As shown in Figure S5b, mass spectrometric curves of CO_2 release further demonstrated that the $CaCO_3$ nanocapsules in situ generated CO_2 major between 600 and 800 °C during the $CaCO_3$@PDA pyrolysis process. At the heating rate of 10 °C min^{-1}, the faster pyrolysis of $CaCO_3$ template, leading to a faster release rate of CO_2. At the heating rate of 5 °C min^{-1}, the release rate of CO_2 appears significantly slowdown from 680 to 750 °C due to more CO_2 reduced to CO during the heat treatment at a lower heating rate. As shown in Figure S5a both TG profiles display similar weight loss from initial temperature to 600 °C. The weight loss is from water evaporation and the thermal decomposition of PDA. The remarkable weight loss between 600 to 800 °C corresponds to the pyrolysis and self-activation processes of the $CaCO_3$. Furthermore, as shown in Table S1, the curve A displays a more weight loss (37.8%) than curve B (30.0%) between 600 to 800 °C, indicating that the slow heating rate of $CaCO_3$@PDA will result in more weight loss. The carbon yield of NPCS-1, NPCS-2, NCS are about 18%, 20% and 24%. These results mentioned above suggest that $CaCO_3$ template self-activation process really can be influenced by different decomposition rate. It indicates the different heating rate may cause different activation results.

Nitrogen (N_2) adsorption-desorption measurements were carried out to investigate the porosities of NPCS-1, NPCS-2 and NCS. As shown in Figure 3a, the isotherms of the NPCS-1 and NPCS-2 are typical IV type isotherms. The isotherms show a rapid

increase at a relative low pressure which is typically associated with micropores. There is an obvious hysteresis loop at relative pressure between 0.45 and 0.9, revealing coexistence of large number of mesopores in NPCS-1 and NPCS-2. A significant increase of the adsorption in the N_2 isotherm of the three samples can be observed at relatively high relative pressure range ($P/P_0 > 0.9$), implying the presence of macropores (causing by removing the template). From the pore size distribution curves (Figure 3b), it is demonstrated that NPCS-1 possesses more mesopores. As shown in Table 1, the pore volume of NCS-1, NPCS-2 and NCS are 1.18, 1.29, and 0.45 $cm^3\ g^{-1}$, and the micropores-contributed pore volume of NPCS-1, NPCS-2, and NCS are 0.23, 0.34 and 0.16 $cm^3\ g^{-1}$, respectively. It is indicated that, compared with NPCS-2, the increased porosity of NPCS-1 is mainly contributed by mesopores. This is because under a slower heating rate, the $CaCO_3$ spheres template has a corresponding slower decomposition rate. Hence, longer activation time is provided which will consequently lead to the wider pores. It proves that the slow heating rate has longer activation time to obtain a larger pore size.

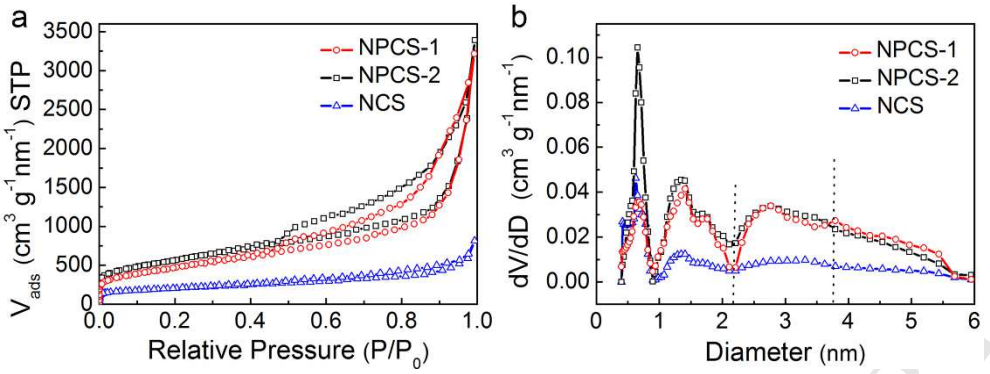

Figure 3. (a) N_2 adsorption-desorption isotherms and (b) corresponding PSDs of NPCS-1, NPCS-2 and NCS.

Table 1. Summary of the physical and chemical characteristics of NPCS-1, NPCS-2 and NCS.

Samples	BET SSA [m^2 g^{-1}]	Pore Volume [cm^3 g^{-1}]	Micro-Pore Volume [cm^3 g^{-1}]	N1s [at. %]	O1s [at. %]
NPCS-1	1692	1.18	0.23	7.57	6.05
NPCS-2	1984	1.29	0.34	5.36	6.36
NCS	684.5	0.45	0.16	3.50	6.51

XPS was performed to analysis the surface nitrogen-containing functional groups. The XPS spectra of NPCS-1, NPCS-2 and NCS were measured and shown in Figure 4a, the nitrogen contents of NPCS-1, NPCS-2 and NCS are 7.57%, 5.36%, 3.50%, respectively. As shown in Figure 4b, the N1s spectra of these three samples are deconvoluted into four binding energies at about 398.5 eV, 400.3 eV, 401.2 eV, 402.9 eV, corresponding to pyridine (N-6), pyridone/pyrrolic nitrogen atoms (N-5),

quaternary (N-Q) and oxidized pyridine nitrogen atoms (N-X). As shown in Figure 4c, NPCS-1, NPCS-2, and NCS have high contents of pyridine (N-6) and pyridone/pyrrolic nitrogen atoms (N-5). These two types of nitrogen are usually considered as the active sites for oxidation and reduction reactions during charge and discharge. The abundant nitrogen-containing functional groups can provide additional pseudocapacitance [38-39].

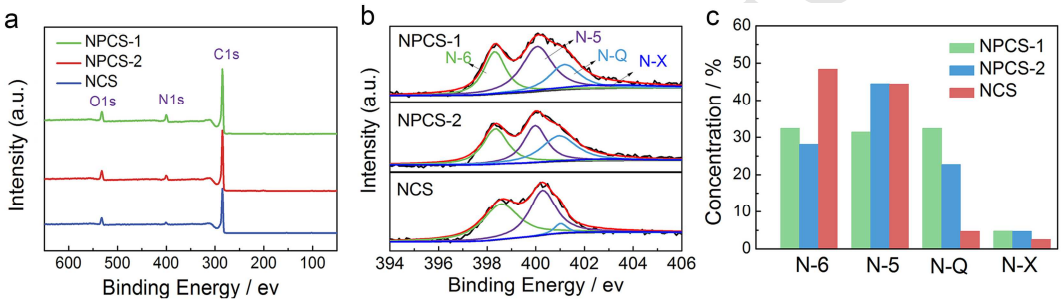

Figure 4. (a) XPS survey spectra. (b) High-resolution N1s spectra. (c) Concentration distribution of different nitrogen groups of NPCS-1, NPCS-2, and NCS.

In order to evaluate the electrochemical performances of NPCS-1, NPCS-2 and NCS materials for EDLC electrodes, these samples were tested in three-electrode system using 6 M KOH electrolyte. As shown in Figure 5a, b, CV curves of NPCS-1, NPCS-2 and NCS electrodes at scan rates of 5 and 100 mV s^{-1} are all quasi-rectangular shapes, the galvanostatic charge/discharge (GCD) curves of these three samples electrodes (Figure 5c, S6) exhibit good symmetry and nearly linear discharge slopes, implying the feature of double electric layer. In addition, NPCS-1

electrode exhibits the longest discharge time, indicating the higher charge storage capability. As shown in Figure 5d, specific capacitances and capacitance retentions at various current densities were recorded. Compared with NPCS-2 (212 F g^{-1}) and NCS (194 F g^{-1}), the capacitance of NPCS-1 is much higher (270 F g^{-1}) at the current density of 0.5 A g^{-1}. Even current density was increased to 20 A g^{-1}, NPCS-1 still retains 70.3% capacitance about 190 F g^{-1}, while the NPCS-2 (142 F g^{-1}) and NCS (88 F g^{-1}) only keep 67.1% and 45.5%, implying that NPCS-1 has an excellent rate performance. Nyquist plots of three samples were presented at a frequency from 0.01 Hz to 100 kHz (Figure 5e). NPCS-1 and NPCS-2 show a more vertical line in low frequency and lower equivalent series resistances in the expanded high frequency region (inset in Figure 5e), indicating that NPCS-1 and NPCS-2 have excellent ion transport performance and electrical conductivity. Additionally, the NPCS-1 also shows an excellent cyclic stability. After 10000 cycles at the current density of 4 A g^{-1}, 97% of the initial capacitance was retained (Figure 5f). As known, EDLC capacitance is from the electrical double-layer formed at the electrode-electrolyte interface, which depends on the accessible surface area of electrodes. The excellent electrochemical performance may attribute to the relatively longer activation time leading to well-balanced meso-, and micro-porosity, which can provide much accessible surface area for electrolyte. Moreover, the nitrogen doping improves the wettability of electrode, resulting in an enhanced ion-accessible area and decreased ion transfer resistance. The samples are abundant in the electrochemically active nitrogen such as

N-5 and N-6. The high content of N-6 and N-5 (electrochemically active) can introduce pseudocapacitance through the faradaic reactions involving protons during the charge and discharge.

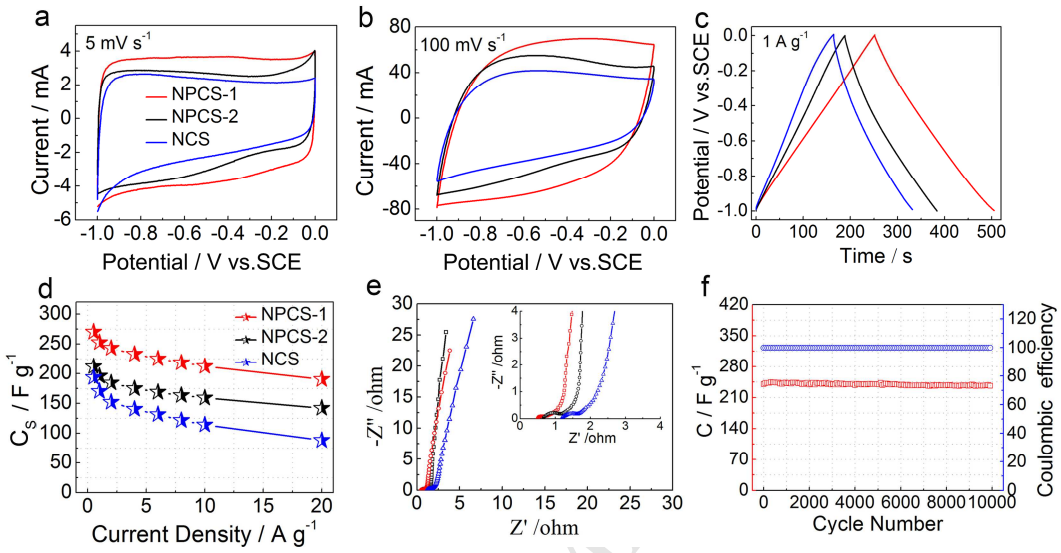

Figure 5. Electrochemical performance of NPCS-1, NPCS-2 and NCS electrodes in the three-electrode system with 6 M KOH electrolyte: CV curves at the scan rate of (a) 5 and (b) 100 mV s^{-1}. (c) GCD curves at the current density of 1 A g^{-1}. (d) Specific capacitances and capacitance retentions at various current densities. (e) Nyquist plots. (f) Cycling performance of NPCS-1 electrode at 4 A g^{-1}.

To explore an in-depth device performance of NPCS-1 electrode, NPCS-1-based EDLC devices were constructed respectively by using 6 M KOH and 5 M LiTFSI aqueous solution as the electrolytes. As shown in Figure S7a, the CV plots of NPCS-1-based EDLC still keep nearly rectangular shapes at the scan rate from 10 to 100 mV s^{-1} in 6 M KOH electrolyte, indicating a good EDLC behavior. All GCD

curves of the symmetrical device (Figure S7c) show symmetrical triangles. The capacitance is about 173 F g^{-1} at the current density of 0.5 A g^{-1}, demonstrating the NPCS-1 has excellent capacitance behavior.

The EDLC device performances of NPCS-1 have also been examined in 5 M LiTFSI. As we all known, the energy density of device is decided by capacitance (C) and voltage (V). In aqueous electrolyte, the maximum cell voltage is 1 V due to the oxygen evolution reaction. By using 5 M LiTFSI aqueous solution as electrolyte, the strong solvation of Li^+ cation can effectively reduce the number of "free" H_2O molecules, simultaneously maintaining the stability of the aqueous electrolyte, enlarging the voltage window of device [40-41]. As shown in Figure S7b, the CV plots of assembled device still keeps nearly rectangular shapes at the scan rate from 10 to 100 mV s^{-1} while its voltage window can be widened to 1.7 V since the presence of over-potential. GCD curves of device (Figure S7d) show symmetrical triangles. The capacitance is about 144 F g^{-1} at the current density of 0.5 A g^{-1}, only a little decrease, compared with 173 F g^{-1} in 6 M KOH electrolyte. As shown in Figure 6c, The NPCS-1-based EDLC tested in 5 M LiTFSI electrolyte could deliver an energy density of 14.4 Wh kg^{-1} at a power density of 427 W kg^{-1} and the 7.8 Wh kg^{-1} at a power density of 8500 W kg^{-1}.

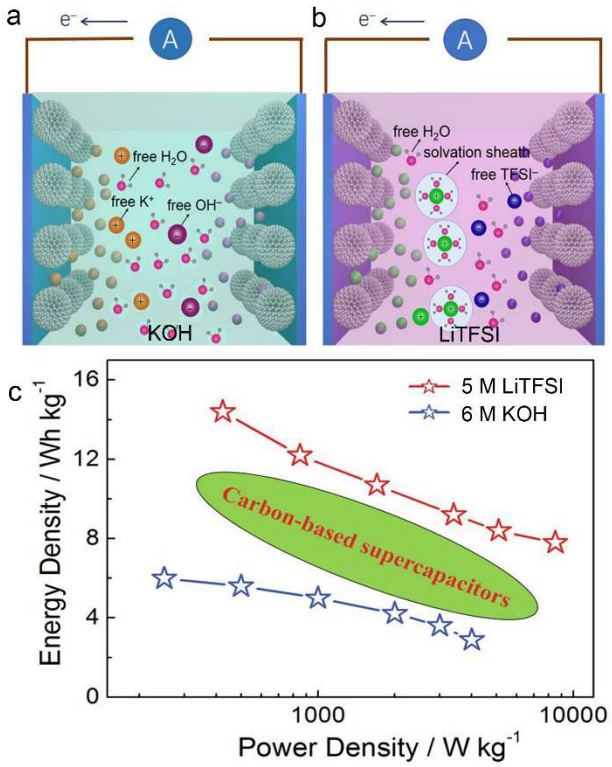

Figure 6. Schematic illustration of the NPCS-1-based EDLC devices by using (a) 6 M KOH and (b) 5 M LiTFSI. (c) Ragone plots of the NPCS-1-based EDLC devices.

4. Conclusions

In conclusion, we report a template-induced self-activation strategy to prepare nitrogen-doped hierarchically porous carbon spheres (NPCS) by using $CaCO_3$ spheres as hard template and activator, dopamine as carbon precursor. The NPCS-1 demonstrates large specific area (up to 1984 m^2 g^{-1}) and high level of nitrogen (N, 7.57%) doping. The electrochemical evaluations in 6 M KOH indicate that the NPCS-1 electrode exhibits gravimetric capacitances of 270 F g^{-1} at 0.5 A g^{-1} and 190 F g^{-1} at 20 A g^{-1}. The cell voltage of the as-assembled EDLC based NPCS-1 electrodes can reach 1.7 V in 5 M LiTFSI, and the gravimetric energy density of 14.4

Wh kg^{-1} can be obtained. The superior performance of NPCS-1 can be attributed to the high surface area, reasonable distribution of micro/mesopores and nitrogen-doping. The high surface area combined with hierarchical pore size distribution not only ensure high ion-accessible surface but also short ion transfer pathway. Furthermore, nitrogen doping improves the wettability of electrode, resulting in enhanced ion-accessible area and decreased ion transfer resistance. Thus, designing self-activation hard templates with a special morphology may be an effective way to obtain a hierarchical carbon with high surface area and well-defined structure.

Acknowledgements

This work was supported by the National Basic Research Program of China (973 Program) (No. 2014CB239701), National Natural Science Foundation of China (No. 21173120, No. 51372116), Natural Science Foundation of Jiangsu Province (BK2011030, BK20151468 and BK20170778) and Priority Academic Program Development of Jiangsu Higher Education Institutions (PAPD).

References and notes

[1]Lukatskaya. M.R, Dunn. B, Gogotsi. Y, Multidimensional materials and device architectures for future hybrid energy storage, Nat. Commun. 7 (2016) 12647.

[2]Gogotsi. Y, Simon. P, True performance metrics in electrochemical energy storage (November, pg 917, 2011), Science 335 (6065) (2012) 167-167.

[3]Simon. P, Gogotsi. Y, Materials for electrochemical capacitors, Nat. Mater. 7 (11)

(2008) 845-854.

[4]Yang. X, Shi. K, Zhitomirsky. I, Cranston. E.D, Cellulose nanocrystal aerogels as universal 3D lightweight substrates for supercapacitor materials, Adv. Mater. 27(40) (2015) 6104-6109.

[5]Zhu. Y.W, Murali. S, Stoller. M.D, Ganesh. K.J, Cai. W.W, Ferreira. P.J, et al. Carbon-based supercapacitors produced by activation of graphene, Science 332 (6037) (2011) 1537-1541.

[6]Wang. Y, Song. Y, Xia. Y, Electrochemical capacitors: mechanism, materials, systems, characterization and applications, Chem. Soc. Rev. 45 (21) (2016) 5925-5950.

[7]Miller. J.R, Simon. P, Materials science, Electrochemical capacitors for energy management, Science 321 (5889) (2008) 651-652.

[8]Wang. F, Wu. X, Yuan. X, Liu. Z, Zhang. Y, Fu. L, et al, Latest advances in supercapacitors: from new electrode materials to novel device designs, Chem. Soc. Rev. 46 (2017) 6816-6854.

[9]Chen. X, Paul. R, Dai. L, Carbon-based supercapacitors for efficient energy storage, Na. Sci. Revi. 4 (3) (2017) 453-489.

[10]Wang. S, Zhang. J, Shang. P, Li. Y, Chen. Z, Xu. Q, N-doped carbon spheres with hierarchical micropore-nanosheet networks for high performance supercapacitors, Chem. Commun. 50 (81) (2014) 12091-12094.

[11]Yuan. C, Liu. X, Jia. M, Luo. Z, Yao. J, Facile preparation of N- and O-doped

hollow carbon spheres derived from poly(o-phenylenediamine) for supercapacitors, J. Mater. Chem. A 3 (7) (2015) 3409-3415.

[12] Zhou. J, Lian. J, Hou. L, Zhang. J, Gou. H, Xia. M, et al, Ultrahigh volumetric capacitance and cyclic stability of fluorine and nitrogen co-doped carbon microspheres, Nat. Commun. 6 (2015) 8503.

[13] Bu. Y.F, Sun. T, Cai. Y.J, Du. L.Y, Zhuo. O, Yang. L.J, et al, Compressing carbon nanocages by capillarity for optimizing porous structures toward ultrahigh-volumetric-performance supercapacitors, Adv. Mater. 29(24) (2017).

[14] Merlet. C, Rotenberg. B, Madden. P.A, Taberna. P.L, Simon. P, Gogotsi. Y, et al, On the molecular origin of supercapacitance in nanoporous carbon electrodes, Nat. Mater. 11 (4) (2012) 306-310.

[15] Zhang. L, Yang. X, Zhang. F, Long. G, Zhang. T, Leng. K, et al, Controlling the effective surface area and pore size distribution of sp^2 carbon materials and their impact on the capacitance performance of these materials, J. Am. Chem. Soc. 135 (15) (2013) 5921-5929.

[16] Ghosh. A, Lee. Y.H, Carbon-based electrochemical capacitors, ChemSusChem 5 (3) (2012) 480-499.

[17] Chmiola. J, Yushin. G, Gogotsi. Y, Portet. C, Simon. P, Taberna. P.L, Anomalous increase in carbon capacitance at pore sizes less than 1 nanometer, Science 313 (5794) (2006) 1760-1763.

[18] Guo. C.X, Li·. C.M, A self-assembled hierarchical nanostructure comprising

carbon spheres and graphene nanosheets for enhanced supercapacitor performance, Energy Environ. Sci. 4 (11) (2011) 4504-4507.

[19] Naveen. M.H, Shim. K, Hossain. M.S.A, Kim. J.H, Shim. Y.B, Template free preparation of heteroatoms doped carbon spheres with trace Fe for efficient oxygen reduction reaction and supercapacitor, Adv. Energy Mater. 7 (5) (2017) 1602002.

[20] Zhang. H, Noonan. O, Huang. X, Yang. Y, Xu. C, Zhou. L, et al, Surfactant-free assembly of mesoporous carbon hollow spheres with large tunable pore sizes, ACS Nano 10 (4) (2016) 4579-4586.

[21] Long. C.L, Chen. X, Jiang. L.L, Zhi. L.J, Fan. Z.J, Porous layer-stacking carbon derived from in-built template in biomass for high volumetric performance supercapacitors. Nano Energy 12 (2015) 141-151.

[22] Chen. C.M, Zhang. Q, Zhao. X.C, Zhang. B, Kong. Q.Q, Yang. M.G, et al, Hierarchically aminated graphene honeycombs for electrochemical capacitive energy storage, J. Mater. Chem. 22(28) 2012 14076-14084.

[23] Guo. D.C, Mi. J, Hao. G.P, Dong. W, Xiong. G, Li. W.C, et al, Ionic liquid C(16)mimBF(4) assisted synthesis of poly(benzoxazine-co-resol)-based hierarchically porous carbons with superior performance in supercapacitors, Energy Environ. Sci. 6(2) 2013 652-659.

[24] Wang. J, Tang. J, Xu. Y, Ding. B, Chang. Z, Wang. Y, et al, Interface miscibility induced double-capillary carbon nanofibers for flexible electric double layer capacitors, Nano Energy 28 (2016) 232-240.

[25] Lee. J, Kim. J, Hyeon. T, Recent progress in the synthesis of porous carbon materials, Adv. Mater. 18 (16) (2006) 2073-2094.

[26] Xing. W, Qiao. S.Z, Ding. R.G, Li. F, Lu. G.Q, Yan. Z.F, et al, Superior electric double layer capacitors using ordered mesoporous carbons, Carbon 44 (2) (2006) 216-224.

[27] Liu. R.L, Shi. Y.F, Wan. Y, Meng. Y, Zhang. F.Q, Gu. D, et al, Triconstituent co-assembly to ordered mesostructured polymer-silica and carbon-silica nanocomposites and large-pore mesoporous carbons with high surface areas, J. Am. Chem. Soc. 128 (35) (2006) 11652-11662.

[28] Lin. T, Chen. I. W, Liu. F, Yang. C, Bi. H, Xu. F, et al, Nitrogen-doped mesoporous carbon of extraordinary capacitance for electrochemical energy storage, Science 350 (6267) (2015) 1508-1513.

[29] Li. H.Q, Liu R.L, Zhao. D.Y, Xia. Y.Y, Electrochemical properties of an ordered mesoporous carbon prepared by direct tri-constituent co-assembly, Carbon 45 (13) (2007) 2628-2635.

[30] Liang. C.D, Dai. S, Synthesis of mesoporous carbon materials via enhanced hydrogen-bonding interaction, J. Am. Chem. Soc. 128 (16) (2006) 5316-5317.

[31] Meng. Y, Gu. D, Zhang. F, Shi. Y, Yang. H, Li. Z, et al, Ordered mesoporous polymers and homologous carbon frameworks: amphiphilic surfactant templating and direct transformation, Angew. Chem. Int. Ed. 117 (43) (2005) 7215-7221.

[32] Deng. Y, Liu. C, Yu. T, Liu. F, Zhang. F, Wan. Y, et al, Facile synthesis of

hierarchically porous carbons from dual colloidal crystal/block copolymer template approach, Chem. Mater. 19 (13) (2007) 3271-3277.

[33] Xu. F, Tang. Z, Huang. S, Chen. L, Liang. Y, Mai. W, et al, Facile synthesis of ultrahigh-surface-area hollow carbon nanospheres for enhanced adsorption and energy storage, Nat. Commun. 6 (2015) 7221.

[34] Wei. W, Ma. G.H, Hu. G, Yu. D, McLeish. T, Su. Z.G, et al, Preparation of hierarchical hollow $CaCO_3$ particles and the application as anticancer drug carrier, J. Am. Chem. Soc. 130 (47) (2008) 15808-1510.

[35] Xu. B, Hou. S, Zhang. F, Cao. G, Chu. M, Yang. Y, Nitrogen-doped mesoporous carbon derived from biopolymer as electrode material for supercapacitors, J. Electroanal. Chem. 712 (2014) 146-150.

[36] Liu. H, Jia. M, Sun. N, Cao. B, Chen. R, Zhu. Q, et al, Nitrogen-rich mesoporous carbon as anode material for high-performance sodium-ion batteries, ACS Appl. Mater & Interfaces 7 (49) (2015) 27124-27130.

[37] Zhao. C, Wang. W, Yu. Z, Zhang. H, Wang. A, Yang. Y, Nano-$CaCO_3$ as template for preparation of disordered large mesoporous carbon with hierarchical porosities, J. Mater. Chem. 20 (5) (2010) 976-980.

[38] Wang. D.W, Li. F, Yin. L.C, Lu. X, Chen. Z.G, Gentle. I.R, et al, Nitrogen-doped carbon monolith for akaline supercapacitors and understanding nitrogen-induced redox transitions, Chem. Eur. J. 18 (17) (2012) 5345-5351.

[39] Hulicova. Jurcakova.D, Seredych. M, Lu. G.Q, Bandosz. T.J, Combined effect of

nitrogen- and oxygen-containing functional groups of microporous activated carbon on its electrochemical performance in supercapacitors, Adv. Funct. Mater.19(3) (2009) 438-447.

[40] Hasegawa. G, Kanamori. K, Kiyomura. T, Kurata. H, Abe. T, Nakanishi K, Hierarchically porous carbon monoliths comprising ordered mesoporous nanorod assemblies for high-voltage aqueous supercapacitors, Chem. Mater. 28 (11) (2016) 3944-3950.

[41] Suo. L.M, Borodin. O, Gao. T, Olguin. M, Ho. J, Fan. X.L, et al, "Water-in-salt" electrolyte enables high-voltage aqueous lithium-ion chemistries, Science 350 (6263) (2015) 938-943.